

# Nanoscale

Accepted Manuscript



This is an *Accepted Manuscript*, which has been through the Royal Society of Chemistry peer review process and has been accepted for publication.

*Accepted Manuscripts* are published online shortly after acceptance, before technical editing, formatting and proof reading. Using this free service, authors can make their results available to the community, in citable form, before we publish the edited article. We will replace this *Accepted Manuscript* with the edited and formatted *Advance Article* as soon as it is available.

You can find more information about *Accepted Manuscripts* in the [Information for Authors](#).

Please note that technical editing may introduce minor changes to the text and/or graphics, which may alter content. The journal's standard [Terms & Conditions](#) and the [Ethical guidelines](#) still apply. In no event shall the Royal Society of Chemistry be held responsible for any errors or omissions in this *Accepted Manuscript* or any consequences arising from the use of any information it contains.

## ARTICLE

# Hollow cobalt phosphonate spherical hybrid as high-efficiency Fenton catalyst†

Cite this: DOI: 10.1039/x0xx00000x

Yun-Pei Zhu,<sup>a</sup> Tie-Zhen Ren<sup>b</sup> and Zhong-Yong Yuan\*<sup>a</sup>Received 00th January 2012,  
Accepted 00th January 2012

DOI: 10.1039/x0xx00000x

[www.rsc.org/](http://www.rsc.org/)

Organic–inorganic hybrid of cobalt phosphonate hollow nanostructured spheres were prepared in an water–ethanol system by using diethylenetriamine penta(methylene phosphonic acid) as bridging molecule, through a mild hydrothermal process in the absence of any templates. SEM, TEM and N<sub>2</sub> sorption characterization confirmed the hollow spherical micromorphology with well-defined porosity. The structure and chemical states of the hybrid materials were investigated by FT–IR, XPS and thermogravimetric analysis, revealing the homogeneous integrity of inorganic and organic units inside the network. As a heterogeneous catalyst, the hollow cobalt phosphonate material exhibited considerable catalytic oxidizing decomposition of methylene blue with sulfate radicals as compared to the cobalt phosphonate nanoparticles synthesized in single water system, which could be ascribed to the enhanced mass transfer and high surface area for the hollow material. Some operational parameters including pH condition and reaction temperature were found to influence the oxidation process. The present results suggest that the cobalt phosphonate material can perform as an efficient heterogeneous catalyst for degradation of organic contaminants, providing insight to the rational design and development of alternative catalysts for wastewater treatment.

## 1. INTRODUCTION

Discharges of industrial wastewaters into the ecosystems have resulted in the contamination of groundwater and thus a series of health and environmental problems. Advanced oxidation processes (AOPs) have emerged as promising strategies for water treatment, especially for persistent and nonbiodegradable pollutants.<sup>1–3</sup> As one of most intensively investigated AOPs, Fenton reaction possesses unique superiorities as an oxidizing process including high degradation efficiency, simple operation, benign process, inexpensive materials and general applicability.<sup>4,5</sup> The classical Fenton reagent is a mixture of hydrogen peroxide (H<sub>2</sub>O<sub>2</sub>) and ferrous ions that catalytically produce active hydroxyl radicals. Although it is considered as an excellent oxidizing agent and is employed in several practical applications, the traditional Fenton reagents still confronted with some considerable limitations. The major constraint is the involvement of highly acidic conditions (pH = 2–3) to prevent the ferrous and ferric ions from hydrolysis. On the other side, the removal of the sludge containing iron ions after neutralization complicates the overall process, making the approach uneconomical.<sup>6</sup> To overcome these disadvantages, other modified Fenton systems have recently testified to be

efficient in organic degradation in wastewater treatment. Manganese-based catalysts involving H<sub>2</sub>O<sub>2</sub> have been developed,<sup>6–9</sup> though their further application is prohibited by the insufficient catalytic performance. Alternatively, cobalt-based Fenton-like systems in the presence of peroxymonosulphate (PMS) have attracted tremendous attention.<sup>10–14</sup> As to the homogeneous reactions, the activation of PMS by cobalt ions leads to the generation of sulfate radicals, which possess more powerful oxidizing ability towards decomposition of organic molecules as compared to hydroxyl radicals, due to the higher standard reduction potential of the reactive radicals.<sup>15–17</sup> Thus, cobalt ions/PMS catalytic systems provide a suitable alternative to convenient Fenton reagent for contaminant oxidation. However, it is noteworthy that the use of cobalt ions in the conventional homogeneous reaction raises a toxicity issue and can further increase the health concern and contribute to increase the pollution. Increasing attention has been paid to develop a heterogeneous catalytic system with incorporated cobalt active sites in a substrate. Some attempts have been reported including cobalt oxides,<sup>18,19</sup> supported cobalt catalysts,<sup>20,21</sup> and cobalt exchanged zeolites<sup>22</sup> as heterogeneous catalysts for activation of PMS. But the general energy-intensive preparation technologies and the insufficient

catalytic activity make them find difficulties in the practical applications.

Synthesis of chemically designed organic–inorganic metal phosphonate hybrid materials represents a significant research direction mainly due to the fact that the adjustment of organophosphonic bridging groups and metallic nodes provides an almost infinite potential to intentionally control the composition in the hybrid network and/or on the surface, leading to various modes of functionalization of the hybrid materials.<sup>23,24</sup> Incorporation of well-defined porosity would further endow metal phosphonates with enhanced performances in the areas of adsorption, separation, and catalysis.<sup>25–27</sup> Noticeably, introduction of multifarious transition metal centers in metal phosphonates can present distinct catalytic activities. For instance, cubic mesoporous titanium phosphonates showed superior photoactivity in degrading organic dyes under simulated solar light irradiation as compared with commercial P25 catalyst.<sup>28</sup> Effective catalytic hydrogenation of 4–nitrophenol to 4–aminophenol under ambient conditions could be achieved through using mesoporous nickel phosphate/phosphonate hybrid microspheres as the catalyst.<sup>29</sup> Mesoporous vanadium phosphonate material constructed from a dendritic tetraphosphonate could perform as excellent catalyst for aerobic oxidation of benzylic alcohols with high reactivity and shape selectivity.<sup>30</sup> Furthermore, after iron was introduced into the micro–mesoporous phosphonate hybrids, the resultant iron phosphonates demonstrated excellent catalytic activity for the synthesis of benzimidazole derivatives under mild liquid-phase reaction conditions, wherein iron centers acted as Lewis acid sites to activate the carbonyl carbon atoms.<sup>31</sup> Our efforts have been focused on the rational synthesis and application exploration of phosphonate-based hybrid materials with fine porous structures.<sup>23,32,33</sup> We reasonably speculated that porous cobalt phosphonate materials could fit the qualification of Fenton reaction for oxidizing organic contaminants, which has been scarcely reported to the best of our knowledge.

It should be noted that heterogeneous catalysts with the similar compositions but different morphologies demonstrate substantially distinct catalytic activities. Nanoparticles have some disadvantages in aqueous reactions such as good dispersion, though powder–like nanoparticles usually suffer from aggregation, deactivation, and difficulty of separation for recycling.<sup>34,35</sup> Solid catalysts of hollow nanostructures have received intensive research interest due to their special properties including large specific surface area, accessible active sites, remarkable delivery ability, and easy settlement, leading to the enhancement of catalytic performance.<sup>36,37</sup> Classical templating strategy to construct hollow structures is efficient, but the further removal of the templates perplexes the fabrication procedures and may result in the collapse of the hollow structures.<sup>38,39</sup> Accordingly, the template-free approach appears to be particularly important.<sup>40,41</sup> However, it remains challenging to prepare hollow nanostructures through a simple way.

Herein, we report a new metal phosphonate hybrid material with well-defined porosity, hollow cobalt phosphonate

nanostructured spheres, which was synthesized under mild hydrothermal conditions using diethylenetriamine penta(methylene phosphonic acid) as the organophosphonic linkage in the absence of any surfactants or templates. The catalytic activity of the resulting cobalt phosphonate as heterogeneous catalyst was tested in the degradation of methylene blue with the assistance of PMS oxidant. The reaction kinetics, thermodynamics and mechanism were investigated and discussed in detail. It was found that the incorporation of cobalt sites and the well-developed porosity appeared to have cooperative effect on the enhanced degradation efficiency.

## 2. EXPERIMENTAL SECTION

### 2.1 Materials synthesis

Diethylenetriamine penta(methylene phosphonic acid) (DTPMP, Henan Qingyuan Chemical Co.) was used as the coupling molecule. In a typical synthesis procedure, 0.4 mmol of DTPMP was dissolved in 25 ml of deionized water, followed by mixing with 5 ml of ethanol. 3 mmol of  $\text{CoCl}_2$  dissolved in 5 ml of water was added slowly under mild stirring and the pH was adjusted by ammonia and HCl to be about 5 after another 4 h of stirring. The obtained mixture was transferred into a Teflon-lined autoclave and aged statically at 140 °C under autogenous pressure for 48 h. The product was filtered, washed with water and ethanol alternatively for several times, and dried at 100 °C. The resultant sample was denoted as S-Co-DTPMP. For comparison, the cobalt phosphonate nanoparticles were also synthesized through the similar procedure while substituting the ethanol with equal amount of water, and the final material was labeled as NP-Co-DTPMP.

### 2.2 Characterization

Fourier transform infrared (FT–IR) spectra were measured on a Bruker VECTOR 22 spectrometer with KBr pellet technique, and the ranges of spectrograms were 4000 to 400  $\text{cm}^{-1}$ . X-ray photoelectron spectroscopy (XPS) measurements were performed on a Kratos Axis Ultra DLD (delay line detector) spectrometer equipped with a monochromatic Al–K $\alpha$  X-ray source (1486.6 eV). All XPS spectra were recorded using an aperture slot of 300 × 700 microns, survey spectra were recorded with a pass energy of 160 eV, and high resolution spectra with a pass energy of 40 eV. Simultaneous thermogravimetry (TG) and differential scanning calorimetry (DSC) were performed using a TA SDT Q600 instrument at a heating rate of 5 °C  $\text{min}^{-1}$  using  $\alpha\text{-Al}_2\text{O}_3$  as the reference. Scanning electron microscopy (SEM) was carried out on a Jeol JSF–7500L at 5 keV. Transmission electron microscopy (TEM) was carried out on a Jeol JEM 2100F at 200 kV. All samples subjected to TEM measurements were ultrasonically dispersed in ethanol and dropcast onto copper grids covered with a carbon film. X-ray diffraction (XRD) patterns were recorded on a Bruker D8 Focus Diffractometer with Cu–K $\alpha$  radiation ( $\lambda = 0.15418$  nm) operated at 40 kV and 40 mA.  $\text{N}_2$  adsorption–

desorption isotherms were measured on a Quantachrome NOVA 2000e sorption analyzer at liquid nitrogen temperature (77 K). The samples were degassed at 100 °C overnight prior to the measurement. The surface areas were calculated by the multi-point Brunauer-Emmett-Teller (BET) method. The chemical compositions of Al and P were analyzed by inductively coupled plasma (ICP) emission spectroscopy on a Thermo Jarrell-Ash ICP-9000 (N + M) spectrometer, and C, N, and H were analyzed on a Vario-EL elemental analyzer.

### 2.3 Degradation experiments

The catalytic activity of the prepared cobalt phosphonate materials was evaluated by the degradation of methylene blue (MB) with the assistance of peroxymonosulfate. Typically, 5 mg of cobalt phosphonate was added in 50 ml of 0.25 mmol L<sup>-1</sup> MB solution, accompanied with magnetic stirring for 1 h to establish adsorption equilibrium. Then the degradation of dye was initiated using peroxymonosulfate (Tianjin Shengmiao Chemical Co.) oxidizing agent with the concentration of 5 mmol L<sup>-1</sup>. Aliquots of the reaction solutions were sampled at designated time intervals during the reaction. The absorbance of reaction solutions was measured using a SP-722 spectrometer at  $\lambda_{\text{max}} = 664$  nm. To evaluate the stability of the catalysts, the sample after one trial was collected through centrifugation, washed by water and ethanol alternatively, and dried for the subsequent cycle test.

## 3. RESULTS and DISCUSSION

### 3.1 Material synthesis and characterization

The synthesis of hollow cobalt phosphonate spheres was performed by the addition of cobalt chloride solution into the mixed solution of ethanol and water of DTPMP, which was followed by a low-temperature hydrothermal process. This would lead to an extended cross-linking reaction between inorganic metallic and organophosphonic precursors. The skeleton structure was investigated by infrared spectroscopy. As shown in Fig. 1, the strong broad band at 3418 cm<sup>-1</sup> and the

sharp band at 1632 cm<sup>-1</sup> are associated with the surface-adsorbed water and hydroxyl groups. Notably, in comparison with the original DTPMP linkage molecule, the bands at 938 and 1138 cm<sup>-1</sup> attributable to the P–OH and P=O stretching vibrations cannot be observed as to the S-Co-DTPMP material, while a new sharp band at 1081 cm<sup>-1</sup> due to P–O–Co vibration can be detected, suggesting the complete condensation of organic and inorganic moieties in the phosphonate hybrid framework.<sup>42</sup> The bands around 500 cm<sup>-1</sup> can be assigned to stretching vibrations of Co–O bonds. The weak band at 1327 cm<sup>-1</sup> can be attributed to C–N stretching, and peaks around 2800–3000 cm<sup>-1</sup> are related to C–H stretching modes of methylene carbon atoms in the organophosphonic linkages. The weak shoulder band located at 1428 cm<sup>-1</sup> can be assigned to P–C vibrations.<sup>43</sup>

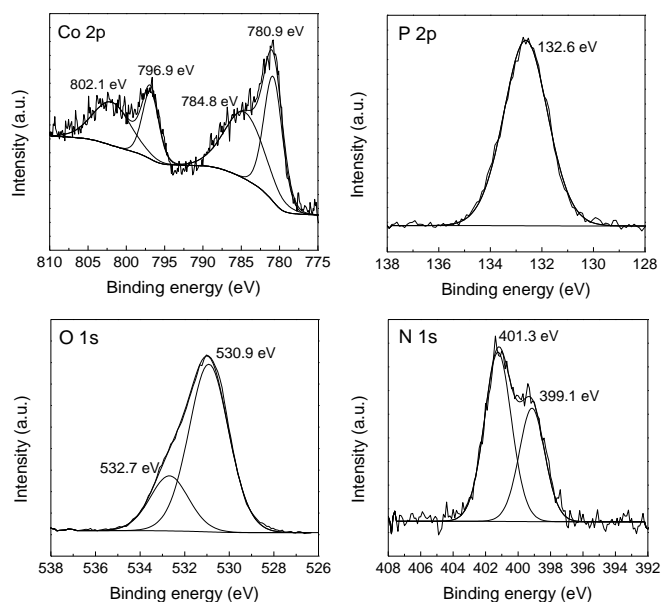


**Fig. 2** High-resolution XPS spectra of Co 2p, P 2p, O 1s and N 1s regions of the S-Co-DTPMP sample.

High-resolution XPS spectrum was taken on the surface of the S-Co-DTPMP sample for the investigation of chemical state and surface stoichiometry (Fig. 2). The binding energies of Co 2p were observed to be 796.9 eV for Co 2p<sub>1/2</sub> and 780.9 eV for Co 2p<sub>3/2</sub>. The spin-orbit splitting value of the 2p peaks is determined to be 16.0 eV, indicating that cobalt elements in the hybrid exists as divalent species.<sup>44</sup> Moreover, the relatively intense satellite peaks at 784.8 and 802.1 eV confirms the presence of Co(II), since mixed-valence just exhibits a weak satellite structure.<sup>45,46</sup> One symmetrical peak of the P 2p spectrum for S-Co-DTPMP was observed at 132.6 eV, which is characteristic of P<sup>5+</sup> in organophosphonate groups. The O 1s lines can be deconvoluted into two components, revealing two kinds of oxygen species. The broad signal at 530.9 eV can be ascribed to the bridging oxygen in the P–O–Co linkages, and a shoulder around 532.7 eV can be assigned to the surface hydroxyl. The N 1s spectrum shows a component at 399.2 eV accompanied with the other one at 401.4 eV, corresponding to

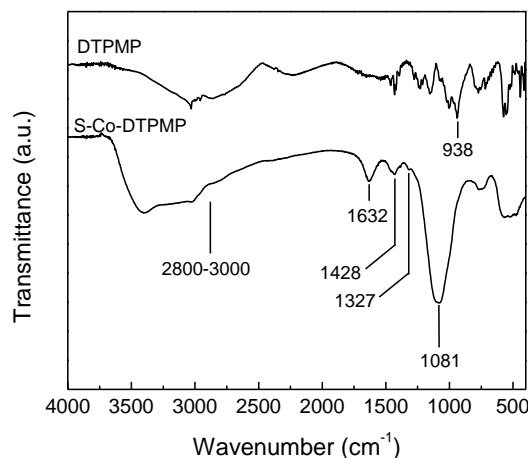


**Fig. 1** FT-IR spectra of DTPMP and the S-Co-DTPMP material.

the bridged N-containing compounds. The surface atomic composition of the cobalt phosphonate material was calculated to be 19.35% Co, 13.21% P, 24.13% C, 35.53% O, and 7.78% N. The surface Co/P ratio was calculated to be 1.46, appropriate to 1.5.

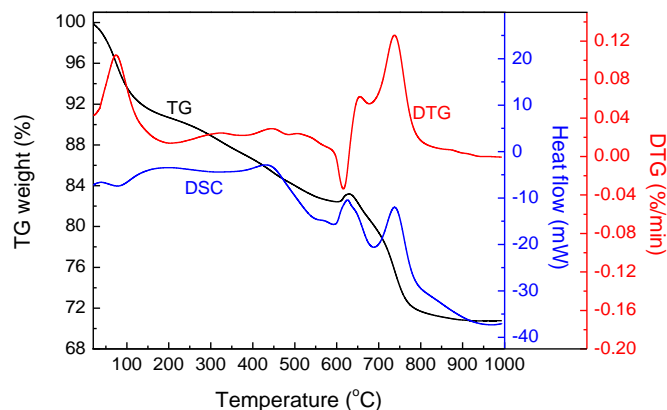


Fig. 3 TG-DSC profiles of the synthesized S-Co-DTPMP sample.

The thermal stability of the organic motifs in the hybrid framework was investigated by the TG–DSC. As shown in Fig. 3, the TG curve presents initial weight loss of 9.2% from ambient temperature to 205 °C, accompanied with an endothermic peak at 82 °C, which may be related to the desorption of adsorbed and intercalated water molecules. The weight loss of 8.4% in the temperature range of 205–600 °C, accompanied with an exothermic peak at around 436 °C, corresponds to the decomposition of organic groups in the hybrid network. Noticeably, a weight gain from 600 to 665 °C can be clearly observed, which can be due to the oxidation of Co(II) to Co(III) in the air atmosphere during the TG test. The third weigh loss from 665 to 910 °C, accompanied with a sharp exothermic peak at about 741 °C, can be related to the combustion of coke. The FT–IR, XPS, and TG–DSC results revealed that no phase separation occurred during the preparation process, and DTPMP bridging groups were homogeneously incorporated into the hybrid network. Combined with ICP emission spectroscopy and the conventional elemental analysis of C, H and N, the S-Co-DTPMP could be formulated as  $\text{Co}_{0.75}(\text{DTPMP}) \cdot x\text{H}_2\text{O}$ .

SEM and TEM observations were employed to characterize the micromorphology of the synthesized cobalt phosphonate materials. It can be seen in Figure 4a that the S-Co-DTPMP material is composed of well-defined microspheres with high yield. These spheres tend to aggregate, which may be due to the resulting high surface energy, and the aggregation may happen primarily during the ripening process.<sup>47</sup> The interior hollow structure is revealed by the broken spheres, as highlighted by arrowheads in Fig. 4a. The detailed morphology of the hollow hybrid microspheres was analyzed by TEM micrographs. As presented in Fig. 4c and e, the pale center and the relatively dark edge indicate the internal chamber property of the cobalt phosphonate material, wherein the hollow hybrid spheres aggregate with each other, leaving considerable macroporosity.

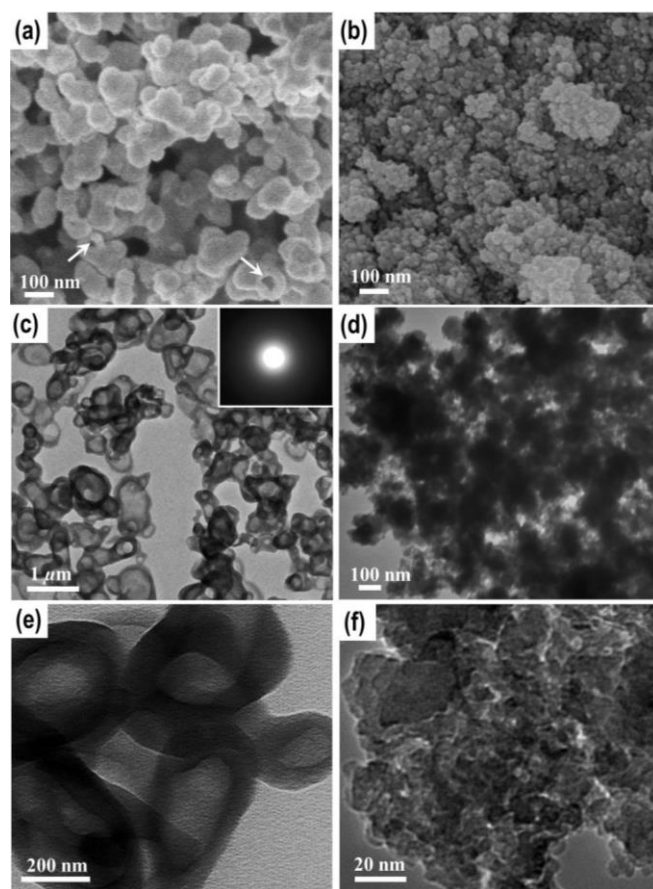


Fig. 4 SEM images of S-Co-DTPMP (a) and NP-Co-DTPMP (b). TEM images of S-Co-DTPMP (c, e) and NP-Co-DTPMP (d, f). The white arrows in (a) state the broken hollow spheres.

On the contrary, the NP-Co-DTPMP sample prepared in the DTPMP aqueous solution are constructed from nanoparticles of tens nanometers (Fig. 4b, d and f). Selected area electron diffraction pattern and wide-angle XRD (Fig. S1, ESI†) confirm that both cobalt phosphonate materials possess amorphous hybrid frameworks.

$\text{N}_2$  sorption analysis was carried out to investigate the architectural porosity of the hybrid materials (Fig. 5). The

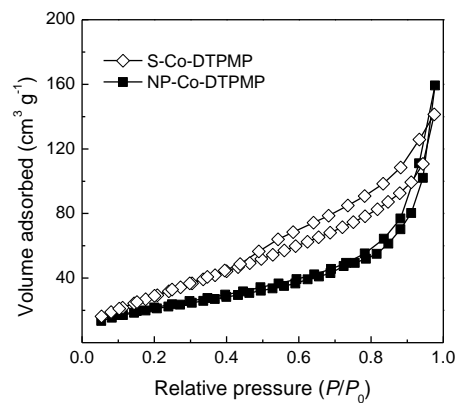


Fig. 5  $\text{N}_2$  adsorption-desorption isotherms of the synthesized cobalt phosphonate materials.

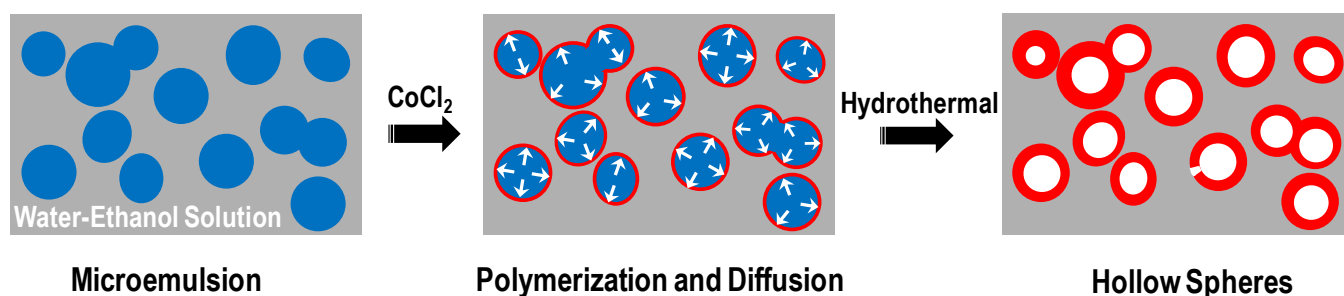


Fig. 6 Formation mechanism of the hollow cobalt phosphonate spheres.

sorption isotherm of S-Co-DTPMP is of between type II and type IV, characteristic of mesoporous structures of fine pore connectivity. The nitrogen volume adsorbed rises steeply at relatively high relatively pressure and do not level off, suggesting the presence of an appreciable amount of secondary porosity of large pores. This is in accordance with the SEM and TEM observation. In the corresponding desorption branch, the isotherm demonstrates a hysteresis loop, which could be due to the existence of mesoporosity originating from the interparticle void spaces. The multi-point BET surface area of S-Co-DTPMP is  $130 \text{ m}^2 \text{ g}^{-1}$ , and the pore volume is  $0.219 \text{ cm}^3 \text{ g}^{-1}$ . The surface area of S-Co-DTPMP is much higher than that of NP-Co-DTPMP ( $86 \text{ m}^2 \text{ g}^{-1}$ ), which implies that different synthesis system could make a difference in the resultant textual properties. It is noteworthy that the utilized organophosphonic precursor DTPMP is water-soluble but alcohol-insoluble (Fig. S2, ESI†), thereby making it flexible under different synthesis conditions. Thus the addition of DTPMP into the water and ethanol mixed solution could give a multiple component system of organophosphonic–water–ethanol, leading to the formation of microemulsion drops under mild stirring (Fig. 6). After introducing cobalt source, the interfacial polymerization between organophosphonic microemulsion and cobalt ions rendered the generation of cobalt phosphonate layers,<sup>48</sup> which could efficiently preserve the initial shape of the microemulsion drops. The subsequent hydrothermal process could accelerate the polymerization reaction and promote the spillover of the emulsions probably due to the distinction of boiling point of water and ethanol, resulting in the formation of broken nanospheres and agminate ones with homogeneously immobilized organophosphonate building units. Since DTPMP was highly soluble in water, only cobalt phosphonate nanoparticles could be obtained through mixing inorganic and organic precursors in the absence of ethanol.

### 3.2 Catalytic activity testing

The simultaneous incorporation of cobalt centers and good porosity in organic-inorganic cobalt phosphonate hybrid inspired us to investigate the catalytic oxidation capability as a Fenton-like heterogeneous catalyst. In order to estimate the reaction kinetics, a general pseudo–first–order kinetics for MB decay could be assumed in the present system:  $\ln(C_0/C) = kt$ ,

where  $C_0/C$  is the normalized organic compound concentration and  $k$  represents the apparent reaction rate constant. The pH condition is an important parameter to influence the catalytic activity. The catalytic performance was evaluated by varying the pH from 2 to 9, and the S-Co-DTPMP was taken as an example. One can see in Fig. 7 that the best degradation efficiency of MB within 25 min can be achieved at neutral pH condition and the corresponding degradation rate is determined to be  $0.136 \text{ min}^{-1}$ . Nevertheless, further decreasing pH value to 5 and 2 causes a notable deterioration of degradation rate to  $0.0331$  and  $0.0203 \text{ min}^{-1}$ , respectively. A reduction of decomposition rate to  $0.0931 \text{ min}^{-1}$  can be observed as well when the pH value is adjusted to 9. This phenomenon is quite different from the case what happened in homogeneous Co(II)/oxone system, of which the Co/oxone process gave almost the same degradation efficiencies throughout the whole pH range of 3 to 8.<sup>13</sup> Indeed, the heterogeneous catalytic reactions are surface processes, where the host-guest interactions are of great significance in affecting the apparent catalytic activities. Under acidic condition, the electrostatic repulsion between the positively charged hybrid surface of cobalt phosphonate<sup>23,49,50</sup> and MB molecules prohibited the effective adsorption process and thus the catalytic degradation. Alkaline condition exhibited lower degradation efficiency in comparison with neutral condition, which may be attributable to that sulfate radicals generated in the reaction system would be quenched by  $\text{OH}^-$ .<sup>51</sup> On the other side, cobalt hydroxide species might be formed on the surface of cobalt phosphonate, arousing the decrease of the catalytic capacity. Thus neutral pH condition was selected as the optimal value for the following catalytic tests. As shown in Fig. 8, no degradation of MB can

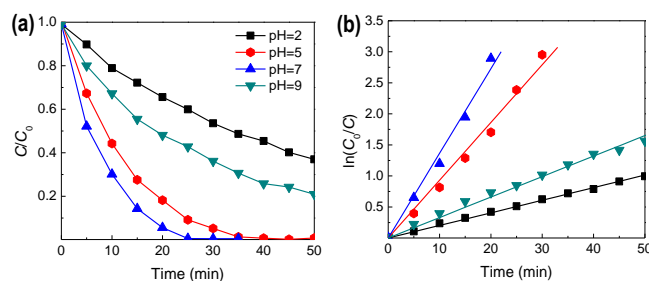
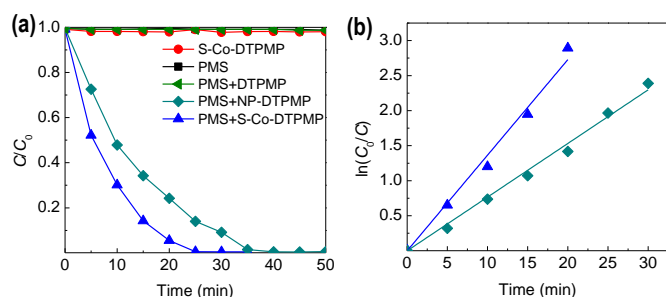


Fig. 7 Catalytic activity of S-Co-DTPMP under different pH conditions. (a) The degradation kinetics of MB, and (b) the linear fitting results by using pseudo–first–order reaction scheme.



**Fig. 8** (a) Degradation kinetic curves of MB using the synthesized cobalt phosphonate materials as catalysts at pH = 7, and (b) the corresponding linear fitting results.

be observed in the presence of PMS alone or PMS and DTPMP. The loss of dye by adsorption is negligible since no obvious concentration variation occurs in the presence of S-Co-DTPMP but without PMS. Furthermore, for the NP-Co-DTPMP catalyst, MB degradation rate ( $0.0766 \text{ min}^{-1}$ ) is lower than that of S-Co-DTPMP and complete degradation can be achieved at 35 min. The enhanced catalytic activity with respect to S-Co-DTPMP could be associated with the larger specific surface area and well-structured porosity, thereby presenting abundant active sites and promoting efficient adsorption and diffusion of reaction molecules so as to improve the catalytic efficiency.<sup>52</sup>

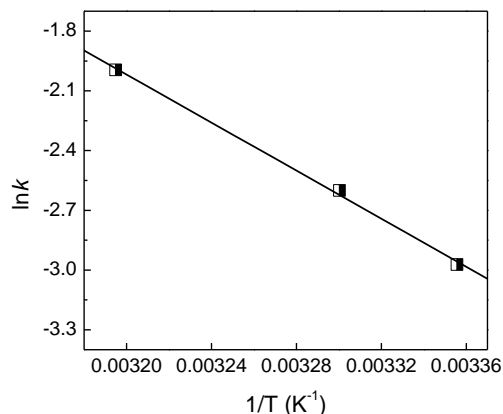
Reusability is a vital standard to weigh a heterogeneous catalyst. Three recycling runs were conducted to evaluate the stability of the S-Co-DTPMP catalyst. As shown in Table 1, the rate of MB oxidation decreases slightly as compared to the fresh catalyst, accompanied with the little decrease of specific area. This may be attributed to the adsorption of contaminants on the hybrid surface. No obvious change of the micromorphology of the catalyst could be observed even after three times cycling tests (Fig. S3, ESI†). The analysis of the solution showed a negligible presence of cobalt ion in the second test and 0.5 ppm cobalt ion leaching in the third run. This implies that the cobalt ion was bonded strongly in the phosphonate hybrid framework, making it quite stable performance in the reaction.

Table 1. Results of catalytic tests using S-Co-DTPMP in different runs

Recycling test	Rate constant / $\text{min}^{-1}$	Surface area / $\text{m}^2 \text{g}^{-1}$
1st use	0.136	130
2nd use	0.132	125
3rd use	0.127	118

Catalytic oxidation reactions were carried out at three different temperatures (25, 30 and 40 °C) to illustrate the corresponding reaction thermodynamics. Fig. 9 shows the effect of reaction temperature on MB removal on S-Co-DTPMP. On the basis of the first-order kinetic model, reaction rate constant at different temperature can be stimulated and the relationship is found to follow the Arrhenius equation:  $\ln k = \ln A + E_a/RT$ , where  $E_a$  is the apparent activation energy,  $R$  is molar gas constant and  $T$  stands for the reaction temperature. The activation energy for this heterogeneous MB disintegration

is calculated to be  $50.2 \text{ kJ mol}^{-1}$ , superior over previously reported cobalt-based heterogeneous catalysts (about  $60 \text{ kJ mol}^{-1}$ ).<sup>10,11</sup>



**Fig. 9** Effect of reaction temperature on MB dye decomposition on the S-Co-DTPMP sample.

In order to identify the primary radical species formed during the oxidation decomposition of MB, quenching experiments were conducted with addition of specific alcohols. The cobalt-mediated activation of peroxydisulfate is known to generate three different radicals including hydroxyl, sulfate and peroxymonosulfate.<sup>53</sup> It is generally considered that alcohols containing alpha hydrogen such as ethanol react at high and comparable rates with hydroxyl and sulfate radicals, and alcohols without alpha hydrogen including *tert*-butyl alcohol exhibit high efficiency in quenching hydroxyl radicals but inefficiency in consuming sulfate radicals. However, peroxydisulfate are relatively inert toward alcohols. According to these properties, the real active radical during the catalytic process can be easily identified through addition of particular alcohols. Fig. 10 demonstrates that the addition of ethanol into the reaction solution results in remarkable decrease of efficiency to 11% even extending the reaction time to 50 min, indicating that the peroxydisulfate radicals could be excluded from being the primary species. Furthermore, the use of *tert*-butyl alcohol can differentiate the roles of hydroxyl and

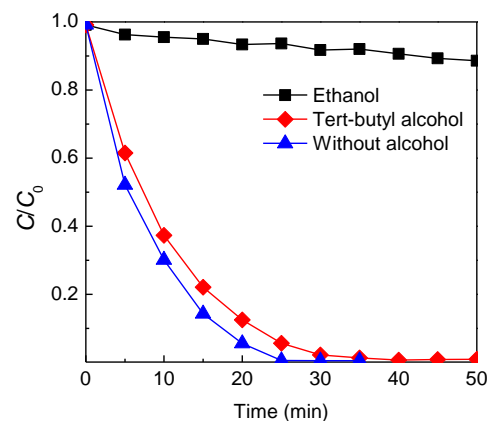


**Fig. 10** Quenching studies for the radical identification by using different alcohols.

sulfate radicals. However, the degradation of MB is slightly affected in the presence of *tert*-butyl alcohol since only 5% reduction in degradation efficiency after 25 min. This means that sulfate radicals are the major oxidizing species formed that are indispensable for the transformation of the substrate.

### 3.3 Discussion

A template-free spontaneous formation process was employed to prepare hollow cobalt phosphonate nanostructured hybrid spheres with homogeneously incorporated organic and inorganic moieties, which was similar to the interfacial emulsion polymerization technique developed for the synthesis of nanoscaled silver hollow spheres and silica nanospheres.<sup>54,55</sup> The distinct solubility of the penta-phosphonic acid in water and ethanol would prompt the formation of microemulsion drops in the multiple component system. The hydrolysis and polymerization between inorganic and organic units might engender microphase-separated domains of cobalt-phosphonate-based layers and water/ethanol/phosphonic cores. Low-temperature autoclaving would accelerate the polycondensation rate and consolidate the framework, endowing the resultant hybrid with favorable thermal stability to 205 °C. It is worthy of noting that the cobalt phosphonate material synthesized in the absence of ethanol were constructed from the aggregated nanoparticles but with relatively lower surface area, which signified that the involved alcohol could efficiently result in spherical micromorphology and the improvement of porosity and textual property of the final cobalt phosphonate samples. For this regard, if the synthesis system was judiciously adjusted such as alcohol species, precursors and reaction temperature, metal phosphonates with well-structured hollow micromorphology could be reasonably prepared, which might find further application potential in the fields of biology and pharmacy besides catalysis.

The high efficiency for the degradation of organic dyes lies primarily in the considerable oxidizing power of the sulfate radicals. It has been shown in the past decades that PMS reagent, generally known as oxone, produces sulfate radicals that are of more powerful oxidizing ability towards decomposition of organic molecules as compared with other oxidants such as hydroxyl radicals.<sup>15,16</sup> This could be related to standard reduction potential of sulfate radicals (2.6–3.1 V) higher than that of hydroxyl counterparts (1.8–2.7 V).<sup>14,17</sup> Also, the divalent cobalt ion has been proven to be the best catalyst for the activation of PMS due to the suitable redox potential.<sup>56</sup> The mechanism of the heterogeneous catalysis is considered to involve a single electron transfer process, the oxidation of Co(II) with peroxymonosulfate and the formation of sulfate radicals as well as the reduction of Co(III) and generation of peroxymononate radicals. The quenching experiments testified that the latter transient species were too weak compared to sulfate ones to induce any degradation of organic dye.

The diffusion, adsorption, reaction and adsorption of guest molecules are typically suggested to be the main steps during a heterogeneous catalytic reaction. Therefore, the incorporation of good porosity with respect to the S-Co-DTPMP sample

could increase the reaction rate due to the improved mass transport through the pore channels and the maintenance of a specific surface area on the level of fine pore systems.<sup>52</sup> Moreover, the pH value of the reaction system had significant influence on the catalytic efficiency, and neutral condition was confirmed to be optimal. The efficient adsorption of MB molecules might be inhibited under acidic condition due to the electrostatic repulsion between the positively charged hybrid surface and organic dyes. However, the alkaline condition could result in the quenching of sulfate radicals and the possible surface passivation by the hydroxide species. The high efficiency at neutral pH value of the oxidation process proposed herewith is a very important advantage for the practical applicability. This is because the pH of the most contaminated natural waters is in the range of 6 to 8. Nonetheless, the classical Fenton reagent should be performed under relatively low pH condition to realize high oxidization capability. The postneutralization and sludge treatment due to the iron species precipitation make the corresponding Fenton system less preferable from the application potential and environmental friendliness point of view. Notably, the synthesized cobalt phosphonate hybrids were firstly attempted to perform as Fenton-like catalysts to the best of our knowledge, exhibiting considerable oxidizing capabilities towards organic contaminants with the assistance of peroxymonosulfate. The experimental results confirmed that the incorporation of hollow nanostructures and cobalt active sites made remarkable contributions to improve the catalytic activities. On the other hand, traditional cobalt-based solid catalysts find difficulties in industrial application owing to the energy-consuming preparation strategies and insufficient activities and stabilities. Herein, the organic-inorganic cobalt phosphonate hybrid materials prepared through a template-free hydrothermal strategy may potentially fulfill the qualifications for the industrial production and application.

### 4. Conclusions

Hollow cobalt phosphonate nanostructured hybrid spheres with good porosity were synthesized in a water–ethanol system through a facile autoclaving method without using any templates or surfactants. The cobalt phosphonate materials possessed amorphous frameworks with alternatively linked cobalt sites and organophosphonic bridging groups, providing abundant active sites for catalytic oxidizing degradation of organic contaminants with the assistance of peroxymonosulfate under ambient conditions. The kinetic study showed that methylene blue decomposition followed pseudo-first-order model with the heterogeneous reaction activation energy of 50.2 kJ mol<sup>-1</sup>, and sulfate radicals were confirmed to be active species. The simple preparation technique and high catalytic activity of the cobalt phosphonate materials make them promising alternative Fenton-like catalysts in environmental remediation.

### Acknowledgements

This work was supported by the National Natural Science Foundation of China (21076056 and 21073099), the Specialized Research Fund for the Doctoral Program of Higher Education (20110031110016), the Program for Innovative Research Team in University (IRT13022), the 111 project (B12015), and the Key Laboratory of Advanced Catalytic Materials in Zhejiang Normal University (ZJHX201301).

## Notes and references

<sup>a</sup> Key Laboratory of Advanced Energy Materials Chemistry (Ministry of Education), Collaborative Innovation Center of Chemical Science and Engineering (Tianjin), College of Chemistry, Nankai University, Tianjin 300071, China. E-mail: zzyuan@nankai.edu.cn.

<sup>b</sup> School of Chemical Engineering and Technology, Hebei University of Technology, Tianjin 300130, China.

† Electronic Supplementary Information (ESI) available: XRD patterns and digital photographs of DTPMP. See DOI: 10.1039/b000000x/

- 1 E. Neyens and J. Baeyens, *J. Hazard. Mater.*, 2003, **98**, 33–50.
- 2 S. H. Tian, Y. T. Yu, D. S. Chen, X. Chen and Y. Xiong, *Chem. Eng. J.*, 2011, **169**, 31–37.
- 3 X. J. Long, Z. Yang, H. Wang, M. Chen, K. Y. Peng, Q. F. Zeng, A. H. Xu, *Ind. Eng. Chem. Res.*, 2012, **51**, 11998–12003.
- 4 J. V. Coelho, M. S. Guedes, R. G. Prado, J. Tronto, J. D. Ardissonc, M. C. Pereirad and L. C. A. Oliveir, *Appl. Catal. B*, 2014, **144**, 792–799.
- 5 P. E. F. Oliveira, L. D. Oliveira and J. D. Ardisson, R. M. Lago, *J. Hazard. Mater.*, 2011, **194**, 393–398.
- 6 G. P. Anipsitakis and D. D. Dionysiou, *Environ. Sci. Technol.*, 2004, **38**, 3705–3712.
- 7 J. Zhao, J. Yang and J. Ma, *Chem. Eng. J.*, 2014, **239**, 171–177.
- 8 C. Yu, G. Li, L. Wei, Q. Fan, Q. Shu and J. C. Yu, *Catal. Today*, 2014, **224**, 154–162.
- 9 Z. Ai, L. Zhang, F. Kong, H. Liu, W. Xing and J. Qiu, *Mater. Chem. Phys.*, 2008, **111**, 162–167.
- 10 P. R. Shukla, S. B. Wang, H. Q. Sun, H. M. Ang and M. Tadé *Appl. Catal. B*, 2010, **100**, 529–534.
- 11 H. Q. Sun, H. Y. Tian, Y. Hardjono, C. E. Buckley and S. B. Wang, *Catal. Today*, 2012, **186**, 63–68.
- 12 N. Oturan, M. H. Zhou and M. A. Oturan, *J. Phys. Chem. A*, 2010, **114**, 10605–10611.
- 13 G. P. Anipsitaki and D. Dionysiou, *Environ. Sci. Technol.*, 2003, **37**, 4790–4797.
- 14 T. Warang, N. Patel, R. Fernandes, N. Bazzanella and A. Miotello, *Appl. Catal. B*, 2013, **132–133**, 204–211.
- 15 J. Fernandez, P. Muruthamuthu, A. Renken and J. Kiwi, *Appl. Catal. B*, 2004, **49**, 207–215.
- 16 P. Raja, M. Bensimon, U. Klehm, P. Albers, D. Laub, L. Kiwi-Minsker, A. Renken and J. Kiwi, *J. Photochem. Photobio. A*, 2007, **187**, 332–338.
- 17 S. K. Ling, S. Wang and Y. Peng, *J. Hazard. Mater.*, 2010, **178**, 385–389.
- 18 Q. Yang, H. Choi, S. R. Al-Abed and D. D. Dionysiou, *Appl. Catal. B*, 2009, **88**, 462–469.
- 19 G. P. Anipsitakis, E. Stathatos and D. D. Dionysiou, *J. Phys. Chem. B*, 2005, **109**, 13052–13055.
- 20 Q. Yang, H. Choi, Y. Chen and D. D. Dionysiou, *Appl. Catal. B*, 2008, **77**, 300–307.
- 21 Q. Yang, H. Choi and D. D. Dionysiou, *Appl. Catal. B*, 2007, **74**, 170–178.
- 22 P. Shukla, S. B. Wang, K. Singh, H. M. Ang and M. O. Tade, *Appl. Catal. B*, 2010, **99**, 163–169.
- 23 Y. P. Zhu, T. Z. Ren and Z. Y. Yuan, *New J. Chem.*, 2014, **38**, 1905–1922.
- 24 J. E. Haskouri, C. Guillem, J. Latorre, A. Beltrán, D. Beltrán and P. Amorós, *Chem. Mater.*, 2004, **16**, 4359–4372.
- 25 T. Kimura and Y. Yamauchi, *Langmuir*, 2012, **28**, 12901–12908.
- 26 T. Kimura, *Chem. Mater.*, 2005, **17**, 5521–5528.
- 27 M. Pramanik and A. Bhaumik, *J. Mater. Chem. A*, 2013, **1**, 11210–11220.
- 28 T. Y. Ma, X. Z. Lin and Z. Y. Yuan, *Chem. Eur. J.*, 2010, **16**, 8487–8494.
- 29 Y. P. Zhu, Y. L. Liu, T. Z. Ren and Z. Y. Yuan, *RSC Adv.*, 2014, **4**, 16018–16021.
- 30 M. Vasylyev and R. Neumann, *Chem. Mater.*, 2006, **18**, 2781–2783.
- 31 A. Dutta, J. Mondal, A. K. Patra and A. Bhaumik, *Chem. Eur. J.*, 2012, **18**, 13372–13378.
- 32 T. Y. Ma and Z. Y. Yuan, *ChemSusChem*, 2011, **4**, 1407–1419.
- 33 Y. P. Zhu, T. Y. Ma, Y. L. Liu, T. Z. Ren and Z. Y. Yuan, *Inorg. Chem. Front.*, 2014, **1**, 360–383.
- 34 C. Yu, J. C. Yu and M. Chan, *J. Solid State Chem.*, 2009, **182**, 1061–1069.
- 35 X. Z. Li, H. Liu, L. F. Cheng and H. J. Tong, *Environ. Sci. Technol.*, 2003, **37**, 3989–3994.
- 36 C. Yu, K. Yang, Y. Xie, Q. Fan, J. C. Yu, Q. Shu and C. Wang, *Nanoscale*, 2013, **5**, 2142–2151.
- 37 C. Yu, F. Cao, X. Li, G. Li, Y. Xie, J. C. Yu, Q. Shu, Q. Fan and J. Chen, *Chem. Eng. J.*, 2013, **219**, 86–95.
- 38 S. W. Kim, M. Kim, W. Y. Lee and T. Hyeon, *J. Am. Chem. Soc.*, 2002, **124**, 7642–7643.
- 39 D. H. W. Hubert, M. Jung, P. M. Frederik, P. H. H. Bomans, J. Meuldijk and A. L. German, *Adv. Mater.*, 2000, **12**, 1286–1290.
- 40 H. J. Hah, J. S. Kim, B. J. Jeon, S. M. Koo and Y. E. Lee, *Chem. Commun.*, 2003, 1712–1713.
- 41 C. H. An, J. Z. Wang, J. X. Liu, S. T. Wang and Y. G. Sun, *ChemSusChem*, 2013, **6**, 1931–1937.
- 42 M. V. Vasylyev, E. J. Wachtel, R. Popovitz-Biro and R. Neumann, *Chem. Eur. J.*, 2006, **12**, 3507–3514.
- 43 X. N. Wei and X. Shi, *J. Phys. Chem. C*, 2014, **118**, 4213–4221.
- 44 M. M. Natile and A. Glisenti, *Chem. Mater.*, 2002, **14**, 3090–3099.
- 45 M. M. Natile and A. Glisenti, *Chem. Mater.*, 2005, **17**, 3403–3414.
- 46 J. Y. Luo, M. Meng, X. Li, X. G. Li, Y. Q. Zha, T. D. Hu, Y. N. Xie and J. Zhang, *J. Catal.*, 2008, **254**, 310–324.
- 47 H. P. Hentze, S. R. Raghavan, C. A. Mckelvey and E. W. Kaler, *Langmuir*, 2003, **19**, 1069–1074.
- 48 X. J. Zhang, T. Y. Ma and Z. Y. Yuan, *Eur. J. Inorg. Chem.*, 2008, 2721–2276.
- 49 A. Cabeza, X. Ouyang, C. V. K. Sharma, M. A. G. Aranda, S. Bruque and A. Clearfield, *Inorg. Chem.*, 2002, **41**, 2325–2333.
- 50 X. Shi, J. P. Liu, Y. Tang and Q. H. Yang, *J. Mater. Chem.*, 2010, **20**, 6495–6504.
- 51 J. Deng, Y. S. Shao, N. Y. Gao, C. Q. Tan, S. Q. Zhou and X. H. Hu, *J. Hazard. Mater.*, 2013, **262**, 836–844.
- 52 Z. Y. Yuan and B. L. Su, *J. Mater. Chem.*, 2006, **16**, 663–677.

## Journal Name

- 53 J. Fernandez, V. Nadtochenko and J. Kiwi, *Chem. Commun.*, 2003, 2382–2383.
- 54 C. Kind, R. Popescu, E. Müller and C. Feldmann, *Nanoscale*, 2010, **2**, 2223–2229.
- 55 S. Schacht, Q. Huo, I. G. Voigt-Martin, G. D. Stucky, and F. Schüth, *Science*, 1996, **273**, 768–771.
- 56 J. Madhavan, P. Maruthamuthu, S. Murugesan and M. Ashokkumar, *Appl. Catal. A*, 2009, **368**, 35–39.